Minería y Geología / v.41 n.1/ january-march / 2025/ p. 51-67 ISSN 1993 8012

ORIGINAL PAPER

Determining ground subsidence using InSAR technology: San Antonio - San Vicente road case study

Determinación de subsidencia del terreno mediante tecnología InSAR. Caso de estudio: Vía San Antonio-San Vicente

Jaime Adrián Peralta-Delgado[1], Luis Enrique Acosta-González[2*], Emil Cristhian Vega-Ponce[1], Walkis Herrera-Blanco[3], Henry Antonio Pacheco-Gil[1]

[1]Technical University of Manabí, Posgrade Faculty, Manabí, Ecuador

[2]University of Holguin, Holguín, Cuba.

[3]University of Moa, Holguín, Cuba.

*Correspondance´Author: luis.acosta.glez@gmail.com

Abstract

This research presents a work scheme for determining ground subsidence using satellite images SENTINEL-1 and processing with SNAP software. Necessary steps for obtaining ground displacements are described, from the download of images in the Copernicus and Alaska platforms to the final export of results in formats that allow an easy interpretation. The San Antonio-San Vicente road, in Manabí (Ecuador) was analyzed as a case study, where the possibility of subsidence in the road infrastructure and surrounding buildings was evident. Displacement values were obtained for 2017-2024 period, using the proposed technological scheme, and graphical tools allowed presenting results that facilitate interdisciplinary analysis and timely decision making. The recorded displacements reached values up to 29 cm, causing cracks in the road structure. These results suggest the existence of a subsidence process in the study area, which is corroborated by visual inspections in several sections of the road, highlighting the importance of satellite monitoring for early detection and management of geological risk in infrastructures.

Keywords: interferometry, SENTINEL-1, displacement estimation, SNAP, InSAR

Resumen

Esta investigación presenta un esquema de trabajo para determinar la subsidencia del terreno mediante el uso de imágenes satelitales SENTINEL-1 y el procesamiento con el software SNAP. Se describen los pasos necesarios para obtener los desplazamientos del terreno, desde la descarga de las imágenes en las plataformas Copernicus y Alaska hasta la exportación final de los resultados en formatos que faciliten su interpretación. Como caso de estudio se analizó la carretera San Antonio-San Vicente, en Manabí (Ecuador), donde se evidenciaba la posibilidad de subsidencia en la infraestructura vial y las edificaciones circundantes. Mediante el esquema propuesto se obtuvieron valores de desplazamiento para el período 2017-2024 y los resultados se presentaron mediante herramientas gráficas que facilitan el análisis interdisciplinario y la toma de decisiones oportunas. Los desplazamientos registrados alcanzaron valores de hasta 29 cm que provocaron grietas en la estructura de la vía. Estos resultados sugieren la existencia de un proceso de subsidencia en la zona de estudio, lo que fue corroborado mediante inspecciones visuales en varios tramos de la carretera, y enfatizan la importancia del monitoreo satelital para la detección temprana y la gestión del riesgo geológico en infraestructuras.

Palabras clave: interferometría, SENTINEL-1, estimación de desplazamientos, SNAP, InSAR

1. INTRODUCTION

Synthetic Aperture Radar Interferometry (InSAR) is a valuable tool used for monitoring and analyzing Earth surface deformations associated with various geological phenomena (ESA, 2017; Palacios, 2019; Braun & Veci, 2021). This technique processes Synthetic Aperture Radar (SAR) images acquired by satellites to obtain precise measurements of surface changes over time. Its ability to cover large areas and provide both historical and up-to-date data makes it an attractive option for researchers, professionals, and organizations involved in environmental, site, and infrastructure monitoring and management.

InSAR technology provides both displacement distribution maps and time series that show the evolution of ground surface and structure displacements over time (Besoya *et al*., 2020; Chen *et al*., 2022; Tomás, 2022; Ruiz-Armenteros *et al*., 2023). As an active remote sensing technique, InSAR has proven to be a versatile and precise tool for detecting ground deformations, making it useful in a wide range of applications, including monitoring hazards such as wildfires, earthquakes, cyclones, and volcanic eruptions. Additionally, it is applied in various fields of Civil Engineering, Geotechnics, and Geomatics,

particularly in infrastructure monitoring (dams, reservoirs, roads, tunnels), mining, railway lines, and slope stability analysis (Xiao *et al*., 2021; Xing *et al*., 2022; Chen *et al*., 2022; Tao *et al*., 2022; Ruiz-Armenteros *et al*., 2023; Piter *et al*., 2024).

InSAR is a methodology that calculates the phase difference between two or more SAR images of the same study area, acquired at different times, to determine topography and/or ground deformation (Guzmán-Acevedo et al., 2020; Tao *et al*., 2022). SAR interferometry relies on a pair of satellite passes to measure phase differences (Martínez-Villar, 2005).

The first acquired SAR image is referred to as the master (reference) image, while the second is called the slave image (Palacios, 2019; Ojeda-Arzuza, 2021). A SAR interferogram is generated by cross-correlating two SAR images, which involves pixel-by-pixel multiplication of the first SAR image with the complex conjugate of the second (Diaz, 2016). The amplitudes of both images are multiplied, and their phases are subtracted to form the interferogram (Guzmán-Acevedo *et al*., 2020).

With the launch of the two SENTINEL-1 satellites (Torres *et al*., 2012; Braun & Veci, 2021), high temporal and spatial resolution SAR data have become freely available. This provides a promising framework for detailed investigations of surface instabilities and large-scale movements with high temporal resolution.

However, it also presents substantial processing challenges due to storage and computational requirements. Efficient methods are needed to detect short-term changes in dynamic environments, requiring approaches that process consecutive scenes to retain maximum temporal resolution for time-series analyses.

Currently, a variety of specialized SAR data processing software products are available, including SNAP (Di-Bisceglie *et al*., 2010; Foumelis *et al*., 2018; Delgado-Blasco *et al*., 2019; Raspini *et al*., 2022), GMTSAR (Sandwell et al., 2011), ISCE (Rosen *et al*., 2012), GAMMA (Yu *et al*., 2019), and SARPROZ (Perissin & Wang, 2011; Hussain, 2022), which are among the most mature and actively developed tools.

This research presents a workflow for estimating ground displacements using SENTINEL-1 satellite images and processing them with SNAP software. The study focuses on a section of the San Antonio–San Vicente road in Manabí, Ecuador, as a case study.

This work is part of the Master's program in Geomatics at the Graduate School of the Technical University of Manabí. The process stages are described, from image downloading to the final export of results in formats that facilitate interpretation and reuse.

2. MATERIALS AND METHODS

The research was conducted on the San Antonio-San Vicente road in Manabí, Ecuador. This area is of particular interest due to documented displacements in the road structure and existing constructions. The study area is located at coordinates: φ = 0°39′ N and λ = 80°18′ W (Figure 1).

Figure 1. Study zone: San Antonio-San Vicente road.

This zone exhibits evident deformations in the Earth's crust. These were identified through visible damage to road infrastructure and buildings, primarily manifested as intense cracking observed during visual inspections. All evidence suggests possible land subsidence in this area (Figure 2).

Figure 2. Detected cracks on the road based in visual inspection (Source: own elaboration).

2.1 Satellite Image Download

The images were obtained in SLC (Single Look Complex) format (Zebker, 2017) from the Alaska Satellite Facility (ASF) platform, available at https://search.asf.alaska.edu (Figure 3).

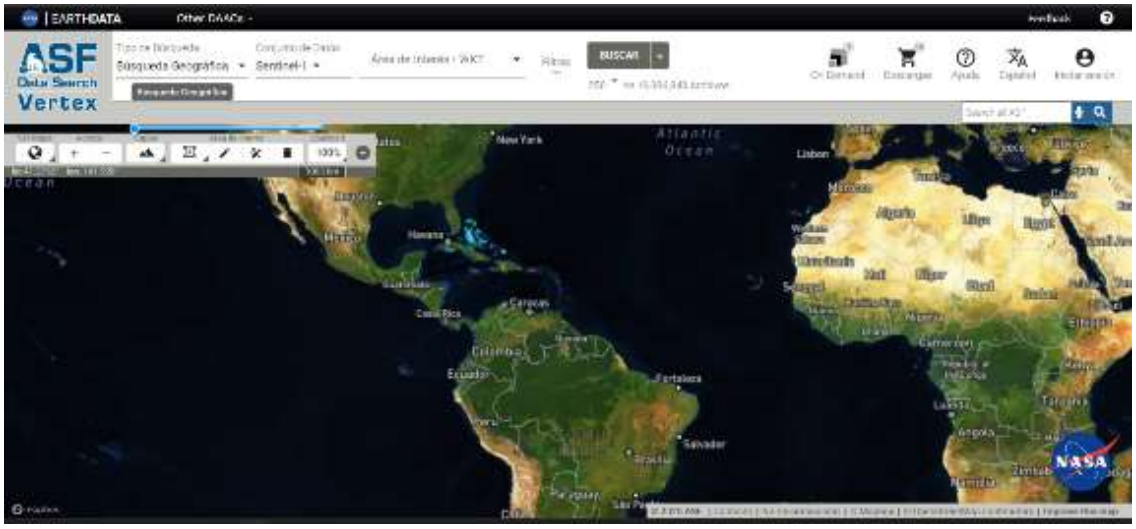

Figure 3. General view of the ASF platform.

Additionally, the Copernicus Open Access Hub platform (https://scihub.copernicus.eu/dhus/#/home) was used to enhance visualization of the study area details and verify the delimitation of the polygon corresponding to the case study (ESA, 2018; Braun & Veci, 2021).

For searching available images in the study area, first a polygon representing the area of interest was defined, and subsequently the corresponding filters were applied (Figure 4).

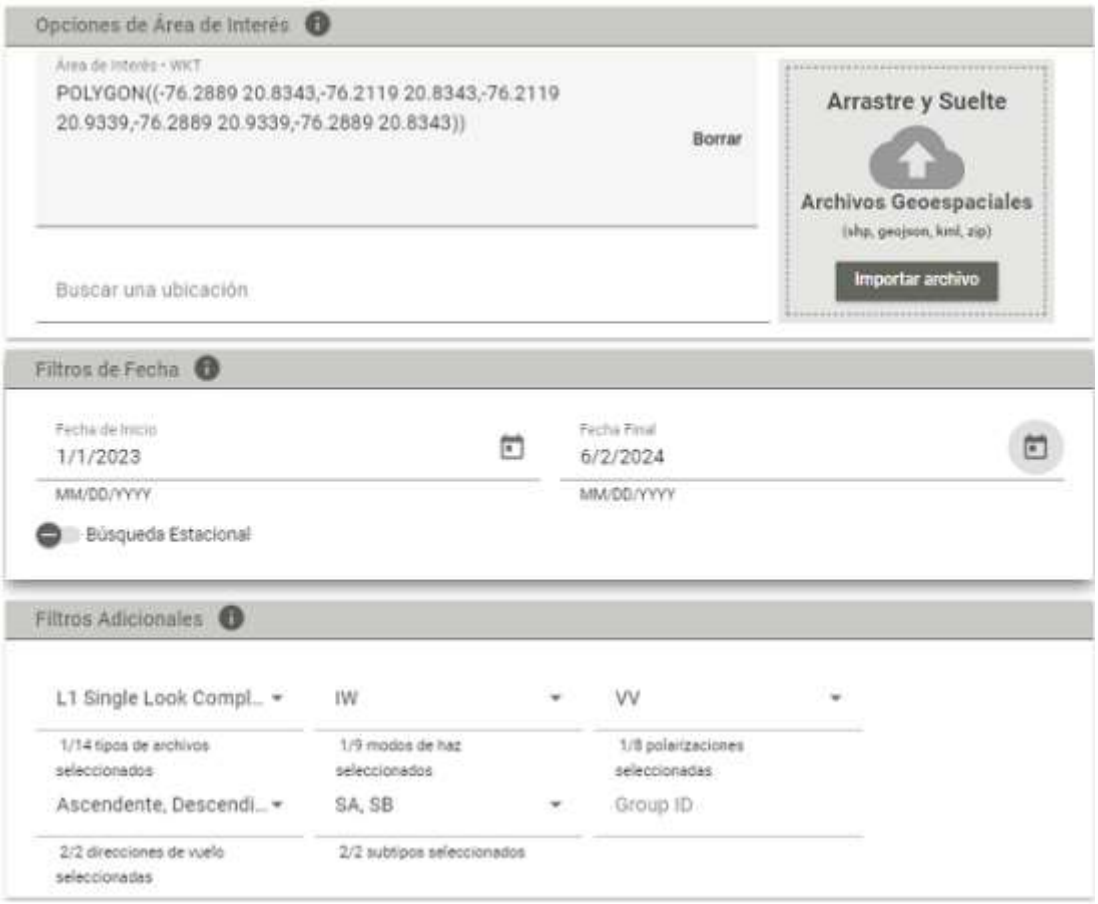

Figure 4. Poligon of the study área and searching filters.

Once the polygon was defined and loaded into the ASF platform, the results of available images in the study area were displayed (Figure 5).

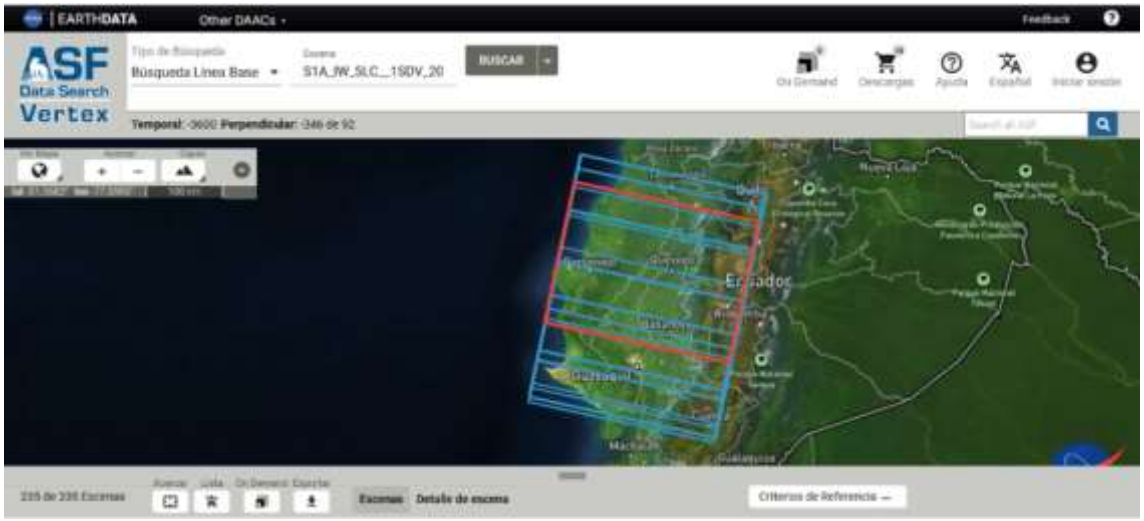

Figure 5. Viewing in ASF of the study zone images.

After completing this operation, the platform shows all available results according to the input parameters. From these, a reference image was

selected and the most suitable pair was chosen through analysis of the Small Baseline Subset (SBAS) technique conditions (Figure 6).

Figure 6. Searching for base line.

For the SBAS search, a reference image of the study area was selected, and the platform identified all secondary scenes matching the spatial coverage. Subsequently, the images were grouped in pairs following chronological order, to facilitate their visualization and selection of the most suitable for the study. Furthermore, a filter was applied establishing a temporal baseline of 12 days, while the perpendicular baseline was maintained at its maximum value (Figure 7).

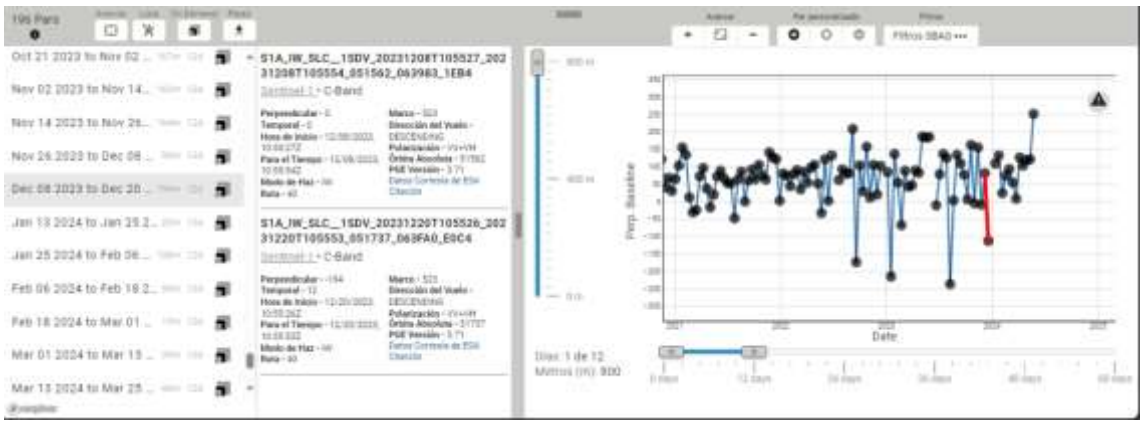

Figure 7. Searching SBAS in the platform ASF.

As a result of the search, the images identified in Table 1 were obtained. These images meet the requirement of having a baseline deviation that does not exceed one meter. Additionally, they present a uniform distribution of time intervals from 2017 to the present date.

Table 1. Denomination of the identified images for the study

imagen ID	Adquisition date	Geographic coordinates (grades)	
		φ	λ
S1A_IW_SLC__1SSV_20150909T110040_20150909T110108_007637_00A966_00DA	2015-09-09	1.83	78.18
S1A_IW_SLC__1SSV_20160224T110032_20160224T110100_010087_00EDCD_C14B	2016-02-24		
S1A_IW_SLC__1SSV_20170424T110052_20170424T110119_010962_010747_782F	2017-04-24		
S1B_IW_SLC__1SSV_20180224T110017_20180224T110044_004441_007BA3_7C5A	2018-02-24		
S1B_IW_SLC__1SDV_20210219T110023_20210219T110050_009691_0117BD_CF35	2021-02-19		
S1B_IW_SLC__1SDV_20240615T110046_20240615T110113_027366_0344BA_E61	2024-06-15		

2.2 Workflow in SNAP

The workflow used is illustrated in Figures 8, 9 and 10 through the graph tool available in SNAP (ESA, 2017; SPA, 2018; ESA, 2021; Mancini, 2021). The operations used to obtain the displacements included: TOPSAR-Split, Apply-Orbit-File, Back-Geocoding, Enhanced-Spectral-Diversity, Interferogram, TOPSAR-Deburst, TopoPhaseRemoval, Multilook, GoldsteinPhaseFiltering, and SnaphuExport.

Figure 8. Scheme used for the first processing in SNAP.

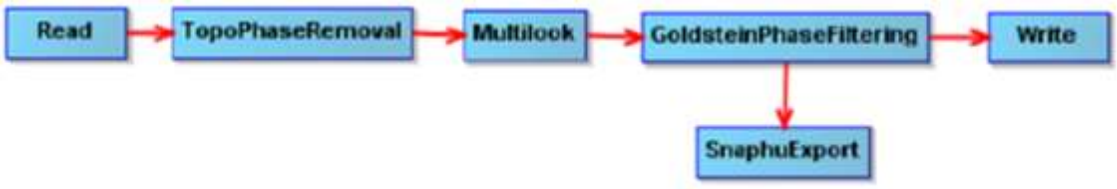

Figure 9. Scheme used for the second processing in SNAP.

The first step (TOPSAR-Split) is part of the image preprocessing, whose objective is to select only the area of interest and thus optimize the computational process. Since the area of interest is contained within three bursts of the SENTINEL-1 image, it is not necessary to process the entire subswath composed of eight bursts. The extraction of bursts in SENTINEL-1's TOPS mode must be performed by acquisition and by subswath. This procedure reduces processing time and is especially recommended when the analysis focuses on a specific area rather than the complete scene.

The processing (Apply-Orbit-File) involves applying orbit files to SENTINEL-1 products, which provides precise information about the satellite's position and velocity. The next step (Back-Geocoding) consists of jointly registering the two SENTINEL-1 images, where the second image (slave) is co-registered with respect to the first (master).

In the Enhanced-Spectral-Diversity step, data from the overlapping area of adjacent bursts is used, followed by range and azimuth correction for each burst. In the next stage (Interferogram), an interferogram is generated between the interferometric pair (master and slave), incorporating a coherence image estimation from the stack of co-registered complex images, with a coherence value of 0.3. Subsequently, in the TOPSAR-Deburst process, images from all bursts in all subswaths are resampled into a common pixel spacing grid in range and azimuth, while maintaining phase information.

The next step involves removing the induced topographic phase from the deburst interferogram (TopoPhaseRemoval). Since the original SAR image contains inherent speckle noise, Multilook processing is applied at this point to reduce the speckled appearance and improve image interpretation. In the GoldsteinPhaseFiltering stage, phase filtering of the interferogram is performed to reduce phase noise, which improves visualization and facilitates the development of the next phase unwrapping step. The final step in this part of the processing is to export the data for SNAPHU Unwrapping processing, with the objective of applying phase unwrapping (ESA, 2017; ESA, 2021; Braun & Veci, 2021).

Figure 10 illustrates the phase unwrapping process. Through this process, a file with the KMZ extension is obtained, which can be opened in Google Earth to visualize the resulting interferogram and subsidence indices in the selected area.

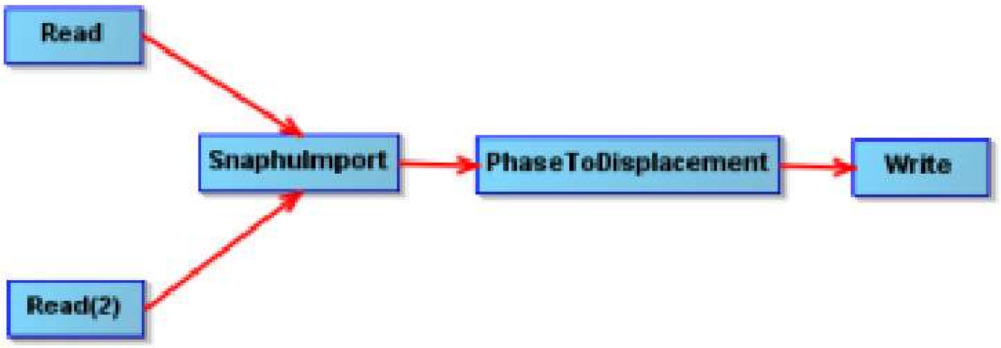

Figura 10. Scheme used to obtain the resulting interferograme.

For displacement to be observable, the coherence must be less than or equal to 0.3. If no displacement is detected, the analyzed images should be replaced as they may contain excessive noise levels.

3. RESULTS AND DISCUSSION

Figure 11 shows the results obtained by applying the previously described workflow, with the generated differential interferograms. This was performed after importing the SNAPHU processing results and constructing the interferometric product, which includes the unwrapped phase band and metadata from the original product. The coherence map is presented in Figure 11(a). Additionally, it is possible to convert the interferometric phase into a displacement map, as shown in Figure 11(b).

Due to topographic variations in the scene and the satellite sensor's inclination, distances may appear distorted in SAR images. For this reason, terrain corrections must be applied to compensate for these distortions, ensuring the geometric representation of the image is as accurate as possible relative to the real world. The result of the corrected displacements is shown in Figure 11(c).

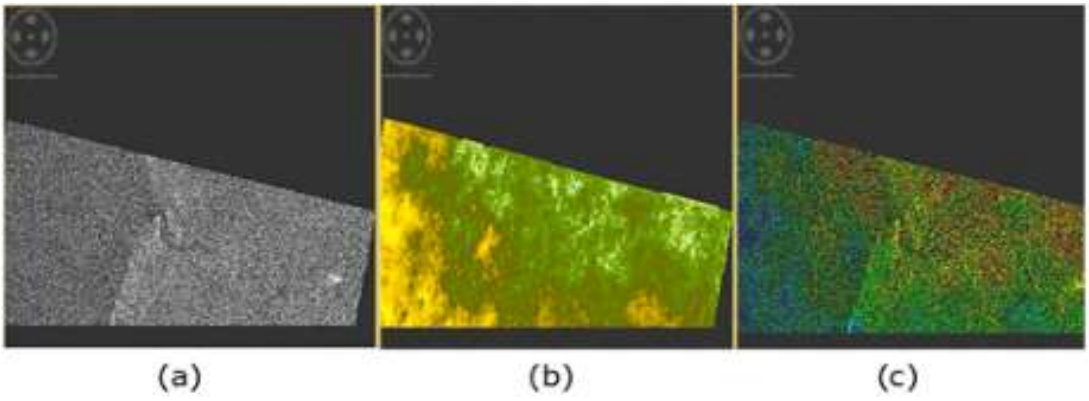

Figure 11. (a) Coherence. (b) Displacements with noises. (c) Displacements with corrections.

For phase unwrapping, the SnaphuImport and PhaseToDisplacement operators were used. Following the application of each step in the described procedure, a new file containing the displacements generated between the master and slave images is obtained. In this file, red-colored areas indicate potential ground subsidence, as shown in Figure 12.

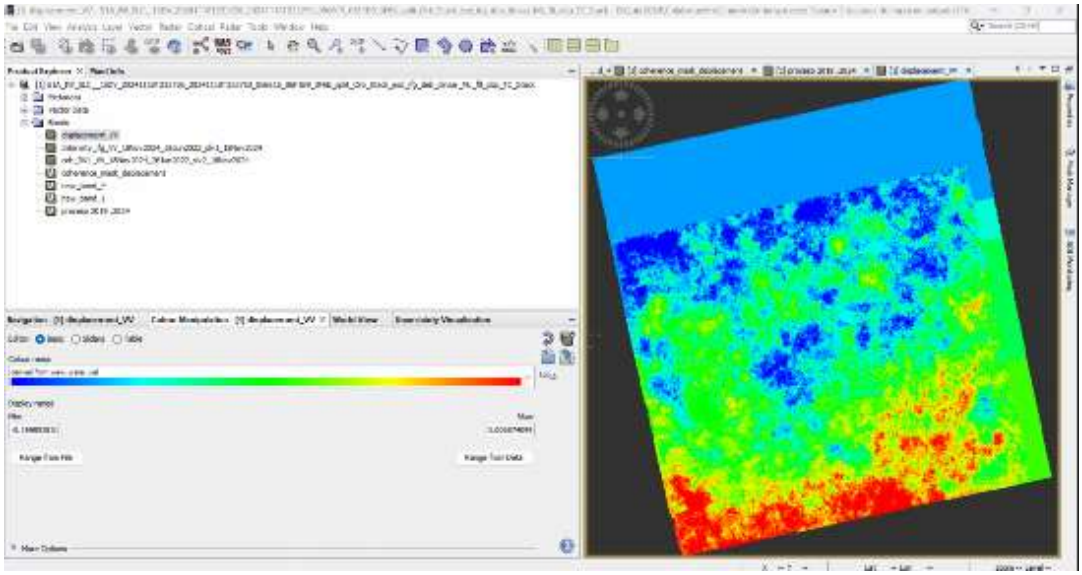

Figura 12. View of displacements generated between the master and slave images.

The displacement results, after removing incoherent values and exporting them for general visualization in Google Earth, are presented in Figure 13.

Figure 13. General view of displacements. *Google Earth*.

Figure 14 displays the displacement map obtained for the study area, calculated from radar images over a two-year period from 2017 to 2019. The displacement values range between 11 cm and 21 cm, with an average value of 16 cm, corresponding to an Earth's crust deformation rate of 8 cm per year.

Figure 14. Results of displacements for the period 2017-2019.

The displacement values obtained for the period from 2019 to 2024 vary between 10 cm and 29 cm, with an average value of 20 cm, corresponding to a deformation rate of 5 cm per year, as shown in Figure 15.

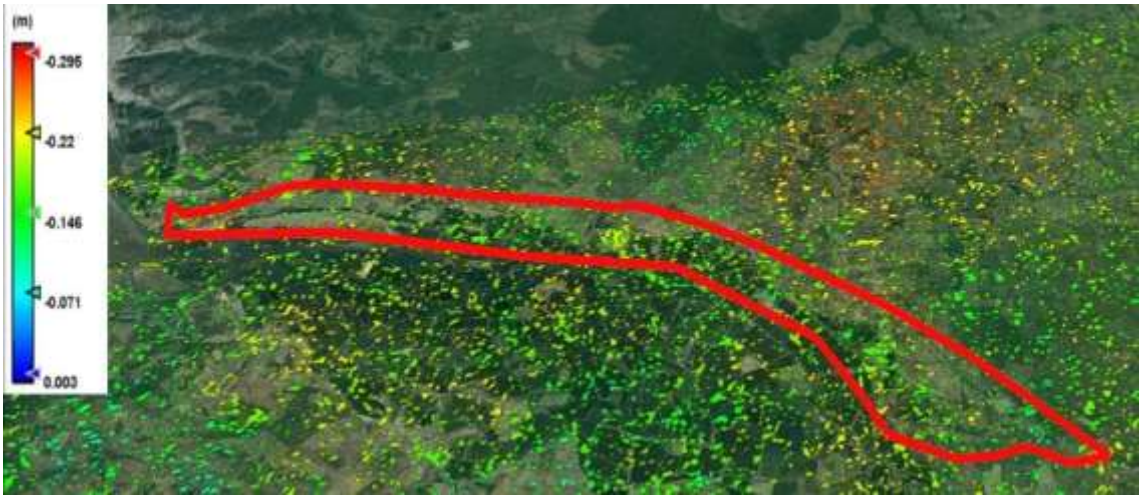

Figure 15. Results of displacements for the period 2019-2024.

The displacements observed in the study area are significant, reaching a maximum value of 29 cm, suggesting possible subsidence in the area. This hypothesis has been corroborated through visual inspections conducted at various sections of the road, where intense cracking and failures in the road substructure were evident, as illustrated in Figure 16.

4. CONCLUSIONS

- The application of SNAP software has proven to be an effective tool for quickly and accurately calculating surface terrain changes using data from open-access platforms. The results obtained can be used to analyze subsidence in new construction areas, as well as to identify zones with higher susceptibility to ground deformations.

- Although integrating SNAP with other specialized programs was not feasible in this case due to the dense vegetation in the study area, the software demonstrated its effectiveness in such scenarios. A significant number of points with sufficient coherence for analysis and interpretation of results were obtained, facilitating timely decision-making regarding the vulnerability of road infrastructure and construction sites. Additionally, SNAP offers advantages in terms of data handling ease, availability of georeferenced information, and generation of graphical displacement visualizations.

- The obtained displacement values suggest the existence of subsidence in the study area, which was corroborated through visual inspections at various sections of the road. During the analyzed period (2017–2024), significant displacements were observed, with magnitudes ranging between 10 cm and 29 cm and Earth's crust deformation rates of up to 8 cm/year. These deformations have led to the appearance of representative cracks in different sections of the road, highlighting the need for continuous monitoring and mitigation measures.

5. ACKNOWLEDGMENTS

The authors acknowledge the collaboration between the following universities: State University of Southern Manabí (UNESUM), Technical University of Manabí (UTM), University of Holguín (UHo), and University of Moa (UMoa), particularly the Geomatics Master's Program of the UTM Graduate School and the Faculty of Technical Sciences, Civil Engineering Program, at UNESUM. Special thanks are extended to MSc. Luis Alberto Ramírez Meléndez from the Faculty of Geology and Mining at UMoa and to Eng. Adrián de la Luz Álvarez Martínez from the Faculty of Engineering at the University of Holguín.

6. REFERENCES

Besoya, M., Govil, H., & Bhaumik, P. (2020). Review on surface deformation evaluation using multitemporal SAR interferometry techniques. Spinger. https://doi.org/10.1007/s41324-020-00344-8.

Braun, A., & Veci, L. (2021). TOPS Interferometry Tutorial.

Chen, Y., Zhang, l., He, Y., Wang, W., & Yang, W. (2022). Ground deformation monitoring and analysis of Zhongchuan International Airport based on the time series InSAR of Sentinel-1A with ascending and descending orbits. Journal of Engineering Geology, 30(3), 803-816.

Delgado-Blasco, J. M., Foumelis, M., Stewart, C., & Hooper, A. (2019). Measuring urban subsidence in the Rome metropolitan area (Italy) with Sentinel-1 SNAP-StaMPS persistent scatterer interferometry. Remote Sensing, 11(2), 129.

Di-Bisceglie, M., Di Santo, M., Galdi, C., Lanari, R., & Ranaldo, N. (2010). Synthetic aperture radar processing with GPGPU. IEEE Signal Processing Magazine, 27(2).

Diaz, D. E. H. (2016). Interferometría radar de apertura sintética (insar) aplicada al estudio del movimiento en laderas aledañas al volcan calbuco con ayuda de imágenes sentinel-1a. Universidad Técnica Federico Santa María, Santiago.

ESA. (2017). InSAR Principles: Guidelines for SAR Interferometry Processing and Interpretation (TM-19, February 2007).

ESA. (2018). LAND SUBSIDENCE WITH SENTINEL-1 using SNAP. https://rus-copernicus.eu/portal/wp-content/uploads/library/education/training/HAZA03_Land-Subsidence_Mexico-city.pdf

ESA. (2021). Sentinel-1 Toolbox. TOPS Interferometry Tutorial. Updated june 2021.

Foumelis, M., Blasco, J., Desnos, Y., Engdahl, M., Fernández, D., Veci, L., & Wong, C. (2018). ESA SNAP-StaMPS integrated processing for Sentinel-1 persistent scatter interferometry. IEEE International Geoscience and Remote Sensing Symposium.

Guzmán-Acevedo, G., Quintana-Rodríguez, J., & Gasca-Zamora, H. (2020). Análisis del potencial de tecnología satelital InSAR para el monitoreo de la infraestructura carretera.

Hussain, M. A., Chen, Z., Shoaib, M., Shah, S. U., Khan, J., & Ying, Z. (2022). Sentinel-1A for monitoring land subsidence of coastal city of Pakistan using Persistent Scatterers In-SAR technique. Scientific Reports, 12(1), 5294.

Mancini, F., Grassi, F., & Cenni, N. (2021). A workflow based on SNAP–StaMPS open-source tools and GNSS data for PSI-Based ground deformation

using dual-orbit sentinel-1 data: Accuracy assessment with error propagation analysis. Remote Sensing, 13(4), 753.

Martínez-Villar, J. (2005). Elaboración y análisis de imágenes radar desde satélite: Monitorización de deformaciones del terreno. Ingeniería Técnica de Telecomunicaciones, Universitat Politénica Catalunya, España.

Ojeda-Arzuza, A. D. (2021). Potencial de la Interferometría de Radar de Apertura Sintética (InSAR) para el análisis del desplazamiento del terreno: caso de estudio Barranquilla, Colombia. Universidad del Norte, Barranquilla, Colombia.

Palacios, D. G. (2019). Aplicación de la interferometría SAR satelital para la detección y monitoreo de los deslizamientos en la carretera escénica Tijuana-Ensenada, BC. (Maestría), Baja California, México.

Perissin, D., & Wang, T. (2011). The SARPROZ InSAR tool for urban subsidence/manmade structure stability monitoring in China. Proceedings of the ISRSE. Sidney, Australia.

Piter, A., Haghshenas-Haghighi, M., & Motagh, M. (2024). Challenges and Opportunities of Sentinel-1 InSAR for Transport Infrastructure Monitoring. PFG–Journal of Photogrammetry, Remote Sensing and Geoinformation Science, 1-19.

Raspini, F., Caleca, F., Del Soldato, M., Festa, D., Confuorto, P., & Bianchini, S. (2022). Review of satellite radar interferometry for subsidence analysis. Earth-Science Reviews, 235, 104239.

Rosen, P., Shams, K., Gurrola, E., Goerge, B., & Knight, D. (2012). InSAR scientific computing environment on the cloud. AGU Fall Meeting Abstract, 2012, IN31C-1508.

Ruiz-Armenteros, A., Delgado-Blasco, J. M., Bakon, M., Lamas-Fernández, F., Marchamalo-Sacristán, M., Gil-Cruz, A. J., ... & Sousa, J. (2023). Monitoring embankment dams from space using satellite radar interferometry: Case studies from RemoDams project. In 5th Joint International Symposium on Deformation Monitoring (JISDM 2022) (pp. 397-404).

Sandwell, D., Mellors, R., Tong, X., Wei, M., & Wessel, P. (2011). Gmtsar: An insar processing system based on generic mapping tools.

SPA, S. I. (2018). Land Subsidence with Sentinel-1 using SNAP. (version 1.2). Retrieved from RUS Lectures at. https://rus-copernicus.eu/portal/the-rus-library/learn-by-yourself/

SNAP. (s.f.). Obtenido de https://step.esa.int/main/

Tao, W., Dai, L., Zhang, Z., Tang, B., & Yu, L. (2022). Stability Analysis Model of Expressway Passing through Goaf Based on SBAS-InSAR Technology. Mathematical Problems in Engineering.

Tomás, R. (2022). Aplicaciones de la interferometría radar de satélite en ingeniería civil. Universidad de Alicante, España.

Torres, R., Snoeji, P., Geudtner, D., Bibby, D., Davidson, M., Attema, E., & Rostan, F. (2012). GMES Sentinel-1 mission. Remote sensing of environment (120).

Xiao, B., Zhao, J., Li, D., Xi, W., Zhou, D., Gao, S., & Zhao, Z. (2021). The Subsidence Detection and Analysis Along Kunming Subway Network Based on SBAS-InSAR. In 2021 28th International Conference on Geoinformatics (pp. 1-8). IEEE.

Xing, X., Zhu, Y., Xu, W., Peng, W., & Yuan, Z. (2022). Measuring Subsidence Over Soft Clay Roads Using a Novel Time-Series InSAR Deformation Model With an Emphasis on Rheological Properties and Environmental Factors (NREM). IEEE Transactions on Geoscience and Remote Sensing, 60, 1-19.

Yu, H., Lan, Y., Yuan, Z., Xu, J., & Lee, H. (2019). Phase unwrapping in InSAR: A review. IEEE Geoscience and Remote Sensing Magazine, 7(1), 40-58.

Zebker, H. (2017). User-friendly InSAR data products: Fast and simple timeseries processing. IEEE Geoscience and Remote Sensing Letters, 14(11), 2122-2126.

Aditional Information

Conflict of interests

The authors declare that there are not conflicts of interest

Author´s Contributions

JADP: Literature review, database work, processing and interpretation of results, writing of the original document. LEAG: Interpretation of results, review of the document, and correction of the final version. ECVP: Review of the original and final versions. WHB: Database work, processing, and interpretation of results. All authors approved the final version of the article submitted for publication.

ORCID

JADP, https://orcid.org/0000-0003-3830-9719
LEAG, https://orcid.org/0000-0002-2723-9850
ECVP, https://orcid.org/0000-0002-2906-8717
WHB, https://orcid.org/0000-0002-6471-0381
HAPG, https://orcid.org/0000-0002-9997-9591

Received: 20/01/2025
Approved: 05/02/2025